Preparation and characterization of porous bioceramic layers on pure titanium surfaces obtained by micro-arc oxidation process

Chi-Sheng Chien[1,2] · Yu-Chien Hung[3] · Ting-Fu Hong[4] · Chung-Chun Wu[3] · Tsung-Yuan Kuo[3] · Tzer-Min Lee[5] · Tze-Yuan Liao[6] · Huan-Chang Lin[7] · Cheng-Hsin Chuang[3]

Abstract Fluorapatite (FA) has better chemical and thermal stability than hydroxyapatite (HA), and has thus attracted significant interest for biomaterial applications in recent years. In this study, porous bioceramic layers were prepared on pure titanium surfaces using a micro-arc oxidation (MAO) technique with an applied voltage of 450 V and an oxidation time of 5 min. The MAO process was performed using three different electrolyte solutions containing calcium fluoride (CaF_2), calcium acetate monohydrate ($Ca(CH_3COO)_2 \cdot H_2O$), and sodium phosphate monobasic dihydrate ($NaH_2PO_4 \cdot 2H_2O$) mixed in ratios of 0:2:1, 1:1:1, and 2:0:1, respectively. The surface morphology, composition, micro-hardness, porosity, and biological properties of the various MAO coatings were examined and compared. The results showed that as the $CaF_2/Ca(CH_3COO)_2 \cdot H_2O$ ratio increased, the elemental composition of the MAO coating transformed from HA, A-TiO_2 (Anatase) and R-TiO_2 (Rutile); to A-TiO_2, R-TiO_2, and a small amount of HA; and finally A-TiO_2, R-TiO_2, CaF_2, TiP_2O_5, and FA. The change in elemental composition was accompanied by a higher micro-hardness and a lower porosity. The coatings exhibited a similar in vitro bioactivity performance during immersion in simulated body fluid for 7–28 days. Furthermore, for in initial in vitro biocompatibility tests performed for 24 h using Dulbecco's Modified Eagle Medium (DMEM) supplement containing 10%Fetal bovine serum, the attachment and spreading of osteoblast-like osteosarcoma MG63 cells were found to increase slightly with an increasing $CaF_2/Ca(CH_3COO)_2 \cdot H_2O$ ratio. In general, the results presented in this study show that all three MAO coatings possess a certain degree of in vitro bioactivity and biocompatibility.

✉ Tsung-Yuan Kuo
tykuo@mail.stust.edu.tw

1 Department of Orthopaedics, Chimei Foundation Hospital, Tainan 710, Taiwan, ROC

2 Department of Electrical Engineering, Southern Taiwan University of Science and Technology, Tainan 710, Taiwan, ROC

3 Department of Mechanical Engineering, Southern Taiwan University of Science and Technology, Tainan 710, Taiwan, ROC

4 Graduate Institute of Materials Engineering, National Pingtung University of Science and Technology, Pingtung 912, Taiwan, ROC

5 School of Dentistry, College of Dental Medicine, Kaohsiung Medical University, Kaohsiung, Taiwan, ROC

6 Quintain steel Company, Tainan 721, Taiwan, ROC

7 Department of Industrial Engineering and Management, I-Shou University, Kaohsiung 84001, Taiwan, ROC

1 Introduction

Titanium (Ti) and its alloys are widely used as biomedical implant materials due to their excellent mechanical properties and corrosion resistance [1]. However, Ti together with its natural oxide thin film TiO_2 is bio-inert. Consequently, chemical bonds are not easily formed between the implant and the surrounding natural tissue, and hence, the osseointegration required to achieve implant longevity is impeded [2]. As a result, the literature contains various proposals for improving the bioactivity of Ti implants through surface modification of the implant itself, or the deposition of thin bioactive films on the implant surface [3–8].

Hydroxyapatite (HA, $Ca_{10}(PO_4)_6OH_2$) is one of the most commonly used materials for implant coatings due to its similarity to bone apatite and excellent osteoconduction and bone regeneration properties. However, bulk HA

is inherently brittle, and cannot, therefore, be used in load bearing applications. Fluorapatite (FA, $Ca_{10}(PO_4)_6F_2$) has the same apatite phase and a similar composition as that of teeth and bones [9]. Thus, as with HA, it also possesses excellent bioactivity. However, compared to HA, FA has a higher interatomic bonding strength, a lower dissolution rate, a better chemical and thermal stability, and a lower bio-resorption tendency [10–12]. As a result, it has many advantages over HA as a biomedical coating material, including an improved physical robustness (i.e., reduced cracking and flaking) and superior corrosion resistance. Due to its excellent osteoconductivity, biocompatibility, and mechanical strength, FA has attracted particular attention as a coating material for dental applications [13–16].

The literature contains many proposals for the preparation of HA coatings, including plasma spraying, sol gel synthesis, pulsed laser deposition, and electrochemical reaction [17–21]. Various studies have shown that micro-arc oxidation (MAO) also provides an effective approach for the deposition of biomedical coatings. In the MAO process, the high-voltage micro-arc discharge events raise the specimen surface instantaneously to a temperature of 2000–3000 °C, causing the surface to melt and regenerate as a thin layer of porous bioactive and biocompatible ceramic material with a high level of wear and corrosion resistance [22–27]. Notably, the MAO process is performed via immersion in an electrolytic bath, and is thus ideally suited to the surface treatment of complex shaped implants. Furthermore, compared with plasma spraying techniques, MAO is simple, easily controlled, and relatively cheap. As a result, it has many practical advantages as a coating technique.

This study utilizes the MAO method to deposit FA porous bioceramic coatings on pure titanium (Cp-Ti) substrates using an electrolyte solution containing three different salts, namely calcium fluoride (CaF_2), calcium acetate monohydrate ($Ca(CH_3COO)_2 \cdot H_2O$), and sodium phosphate monobasic dehydrate ($NaH_2PO_4 \cdot 2H_2O$). The investigation focuses specifically on the effects of the electrolyte concentration and composition on the surface morphology, elemental composition, micro-hardness, porosity, and biological properties of the MAO coatings.

2 Experiments

As described above, the MAO deposition process was performed using an electrolyte solution containing a mixture of CaF_2, $Ca(CH_3COO)_2 \cdot H_2O$ and $NaH_2PO_4 \cdot 2H_2O$. Three different electrolyte solutions were prepared with CaF_2/$Ca(CH_3COO)_2 \cdot H_2O$/$NaH_2PO_4 \cdot H_2O$ ratios of 0:2:1 (0%F), 1:1:1 (33%F), and 2:0:1 (67%F), respectively (see Table 1). The Cp-Ti substrates were machined into dimensions of

Table 1 MAO electrolyte composition and concentration

Specimen	Electrolyte solutions		
	CaF_2	$Ca(CH_3COO)_2 \cdot H_2O$	$NaH_2PO_4 \cdot 2H_2O$
0%F	0 M	0.26 M	0.12 M
33%F	0.13 M	0.13 M	0.12 M
67%F	0.26 M	0 M	0.12 M

20 mm × 20 mm × 3 mm, ground using 1200-grit SiC paper, and then cleaned in acetone and ethanol. In performing the MAO process, the substrates were anodized with a DC power supply and a stainless steel plate was placed at a distance of approximately 10 mm from the substrate to serve as a cathode. In every case, the applied voltage was set as 450 V, the oxidation time as 5 min, and the electrolyte temperature as 20 °C. (Note that a low electrolyte temperature was deliberately chosen to minimize the safety risk posed by the spark/arc discharges produced during the deposition process.) Following the MAO process, the specimens were cleaned ultrasonically in de-ionized (DI) water for 15 min.

The microstructures of the various coatings were observed using scanning electron microscopy (SEM, JEOL JSM-6390LV, JEOL Ltd., Tokyo, Japan). In addition, the porosity was evaluated using commercial Image Pro Plus 5.0 software. The compositions and phases of the different coatings were analyzed by energy dispersive X-ray spectrometry (EDS) and X-ray diffraction (XRD, Cu Kα radiation, Rigaku D/Max Ⅲ.V, Rigaku Ltd., Tokyo, Japan), respectively. In addition, the hardness of the coatings was determined using a micro-Vickers hardness tester under a maximum indentation load of 300 g. The hardness measurements were taken in such a way as to avoid the pore regions on the coating surface. Moreover, for each coating, three specimens were taken; with the results, then averaged to obtain a single representative value for the sample.

The in vitro bioactivity performance of the various coatings was evaluated by soaking the specimens in simulated body fluid (SBF) for 7, 14, 21, and 28 days at a temperature of 37 ± 0.1 °C. The SBF solution was prepared by dissolving reagent-grade NaCl, $NaHCO_3$, KCl, $K_2HPO_4 \cdot 3H_2O$, $MgCl_2 \cdot 6H_2O$, $CaCl_2$, and Na_2SO_4 in distilled water. The inorganic ion concentrations of the SBF solution and human blood plasma, respectively, are listed in Table 2. Prior to immersion in the SBF, the specimens were cleaned ultrasonically in DI water for 10 min and then sterilized at a temperature of 120 °C for 20 min. Following the immersion tests, the phases within the coatings were identified using XRD with a 2θ scanning range of 20°~60° and a scanning rate of 4° min^{-1}.

Finally, the in vitro biocompatibility performance of the coatings was briefly assessed by examining the spreading and attachment of osteoblast-like osteosarcoma MG63 cells

Table 2 Inorganic ion concentrations of SBF and human blood plasma

(mM)	Na^+	K^+	Ca^{2+}	Mg^{2+}	Cl^-	HCO_3^-	HPO_4^{2-}
SBF	142.0	5.0	2.5	1.5	148.8	4.2	1.0
Blood	142.0	5.0	2.5	1.5	103.0	27.0	1.0

on the coating surface. The MG63 cells were first digested by trypsin to form cell suspensions. The suspensions (pre-incubated cells) were then seeded with a cell density of 5×10^3 (cells/cm^2) on coating specimens contained in 24-well plates. The plates were cultured with Dulbecco's Modified Eagle Medium (DMEM) supplement containing 10%Fetal bovine serum in a humidified incubator with 5% CO_2 at 37 °C for 24 h. Following the culturing process, the DMEM solution and non-adherent cells were removed from the specimen surface by washing three times with phosphate-buffered saline (PBS). Subsequently, the viable cells were fixed using PBS containing 2.5 vol.% glutaraldehyde, serially dehydrated using ethanol with an incrementally increasing concentration (30, 50, 70, 95 and 100%), and then critical-point-dried in hexamethyldisilazane (HMDS) for 10 min. The morphologies of the cells attached to the various coating specimens were then observed by SEM.

3 Results and discussion

3.1 Surface morphology and phase identification of MAO coatings

Figure 1a–c show the SEM surface morphologies and EDS analysis results for the coatings prepared in electrolyte solutions with 0%F, 33%F, and 67%F, respectively. It is seen that all of the specimens have a porous microstructure with micropores resembling craters on mountaintops formed as a result of the multiple micro-arc discharge events [28]. For the 0%F specimen, the coating has a porosity of approximately 12% and most of the micropore diameters lie in the range of 1–2 μm. By contrast, the 33%F specimen has a slightly lower porosity of 11% and a larger pore diameter (3–5 μm). Finally, the 67%F specimen has a low porosity of just 2% and only a very small number of micropores (Fig. 1c). The low porosity of the 67%F coating suggests that the greater quantity of CaF_2 in the electrolyte solution cannot be fully dissolved. As a result, micro-arc discharge-decay occurs, leading to a dramatic reduction in the dielectric breakdown effect and electrochemical reaction at the Ti surface during the MAO process. Porous layers produced on the MAO sample surfaces can provide several advantages for long-term clinical performances. The porous structure allows cell adhesion and maintain cell growth. The following new form tissue is able to grow into

the pores and lock the artificial implant for greater mechanical stability at this critical interface [29, 30].

Figure 2a–c shows SEM cross-sectional micrographs of the three MAO coatings on the Ti substrates. The 0%F, 33%F, and 67%F coatings have average thicknesses of 20, 15, and 130 μm, respectively. Compared to the electrolyte solution for the 0%F coating, that for the 33%F coating contains less $Ca(CH_3COO)_2 \cdot H_2O$ (which promotes HA formation) and more CaF_2 (which impairs the electric conductivity/solubility). Thus, the oxide layer on the 33%F specimen has a lower thickness than that on the 0%F specimen, since, as the electric conductivity of the electrolyte solution decreases, the number of electron avalanches also decreases and hence a micro-arc discharge-decay effect occurs [31]. For the 67%F specimen, the $Ca(CH_3COO)_2 \cdot H_2O$ in the electrolyte solution is totally replaced by CaF_2, and hence the electric conductivity of the solution is due mainly to the $NaH_2PO_4 \cdot H_2O$ content. As a result, the micro-arc discharge phenomenon is suppressed during the MAO process and hence continuous growth of the oxide layer occurs under the effects of anodic oxidation. For this particular specimen, the voltage is limited to a maximum value of 300 V due to the lower electrical conductivity of the electrolyte. As a result, some of the CaF_2 in the electrolyte solution is not dissociated into ion form, and the electric conductivity of the solution is thus reduced. However, CaF_2 is still absorbed onto the specimen surface by the electrophoretic deposition during the MAO process (as confirmed by the XRD results) [32]. Consequently, a significant increase in the oxide layer thickness occurs.

Figure 3 shows the EDS surface mapping results for the three MAO coatings. The results show that in addition to Ti, the surfaces mainly consist of Ca, P, C, and O (see also the EDS analysis results in Fig. 1). It is observed that the F content of the coatings increases from 0 at.-% to 7.54 at.-% with an increasing $CaF_2/Ca(CH_3COO)_2 \cdot H_2O$ ratio. In other words, the Ca and P ions in the electrolyte solution are compounded into the oxide film during the MAO process. The previous studies have reported that porous films containing Ca and P ions promote bonding between the implant and surrounding bone tissue, since the ions serve as anchorage points [26, 33]. The results presented in Fig. 3 show that while the F and P contents of the coatings increase with an increasing $CaF_2/Ca(CH_3COO)_2 \cdot H_2O$ ratio, the Ca content reduces.

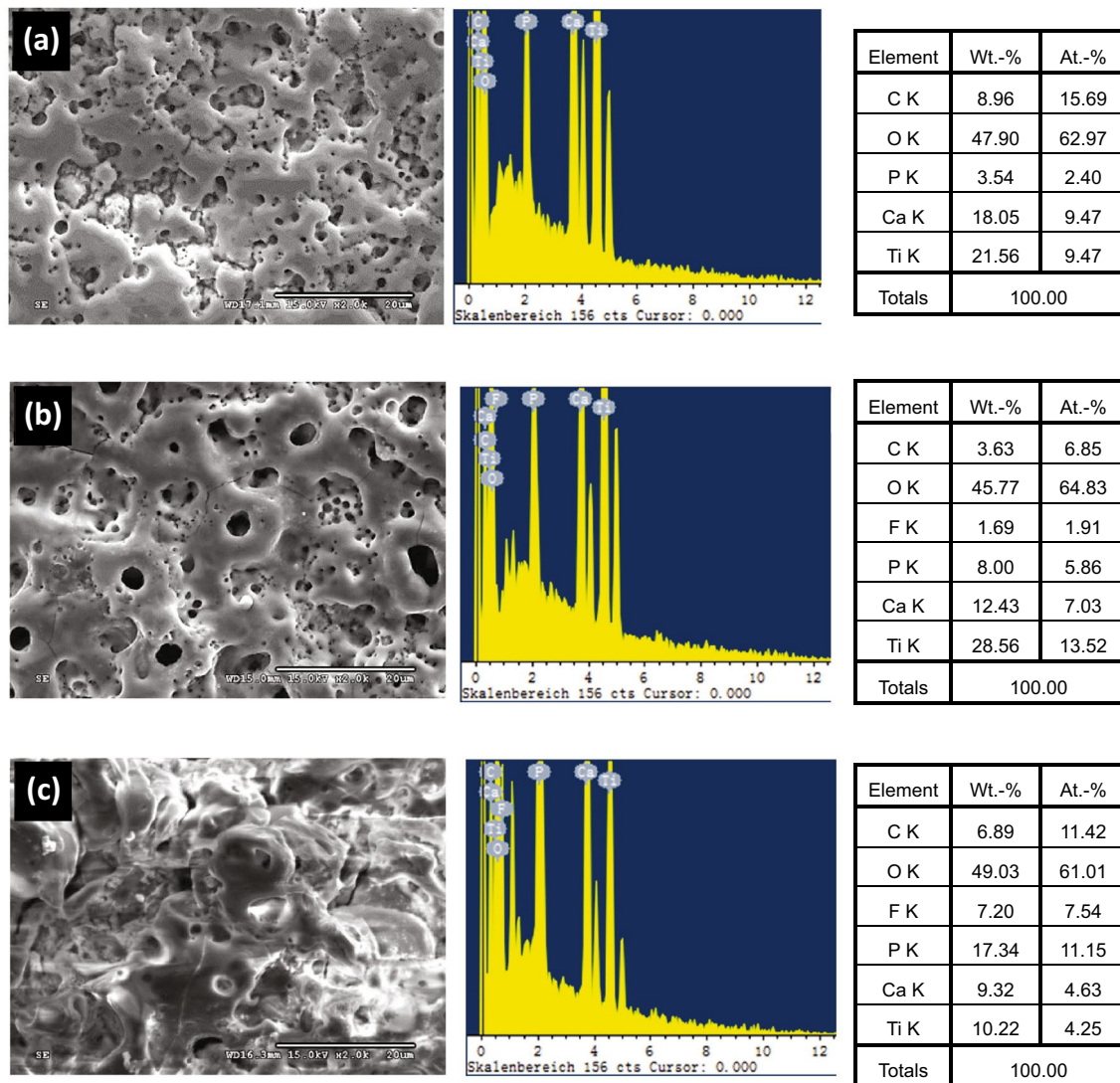Figure 4 shows the EDS line scan results for the composition profiles through the coating thickness. It is seen

Element	Wt.-%	At.-%
C K	8.96	15.69
O K	47.90	62.97
P K	3.54	2.40
Ca K	18.05	9.47
Ti K	21.56	9.47
Totals	100.00	

Element	Wt.-%	At.-%
C K	3.63	6.85
O K	45.77	64.83
F K	1.69	1.91
P K	8.00	5.86
Ca K	12.43	7.03
Ti K	28.56	13.52
Totals	100.00	

Element	Wt.-%	At.-%
C K	6.89	11.42
O K	49.03	61.01
F K	7.20	7.54
P K	17.34	11.15
Ca K	9.32	4.63
Ti K	10.22	4.25
Totals	100.00	

Fig. 1 Surface morphology and EDS analysis results for coatings prepared using electrolyte solutions with **a** 0%F, **b** 33%F, and **c** 67%F

Fig. 2 SEM cross-sectional views of coated Cp-Ti specimens prepared using electrolyte solutions with **a** 0%F, **b** 33%F, and **c** 67%F
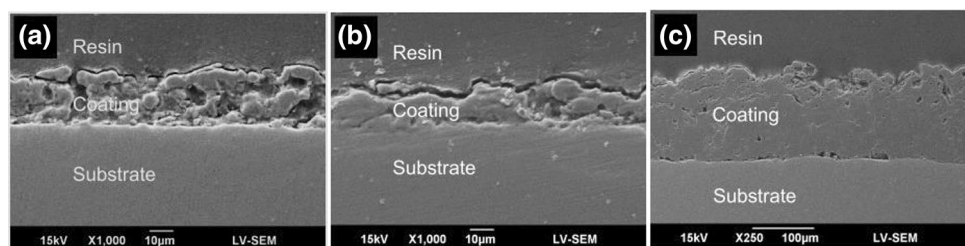
that the Ca content decreases and the P, O, and F contents increase as the $CaF_2/Ca(CH3COO)_2 \cdot H_2O$ ratio in the electrolyte solution increases (i.e., 0%F→33%F→67%F). In other words, the change in composition of the coatings is consistent with the change in composition of the electrolyte solution. (It is hence inferred that most of the elements in the electrolyte solution react to form the oxide layer.) In addition, it is seen that the 67%F coating has a lower overall Ca content than the other two coatings, but a higher Ca and F content at the outer surface. This is thought to be related to the particular characteristics of the mixed FA and CaF_2 deposition process.

A close inspection of the EDS analysis results of coating surface presented in Fig. 1 shows that the Ca/P ratio

Fig. 3 EDS mapping results of coatings prepared using electrolyte solutions with **a** 0%F, **b** 33%F, and **c** 67%F
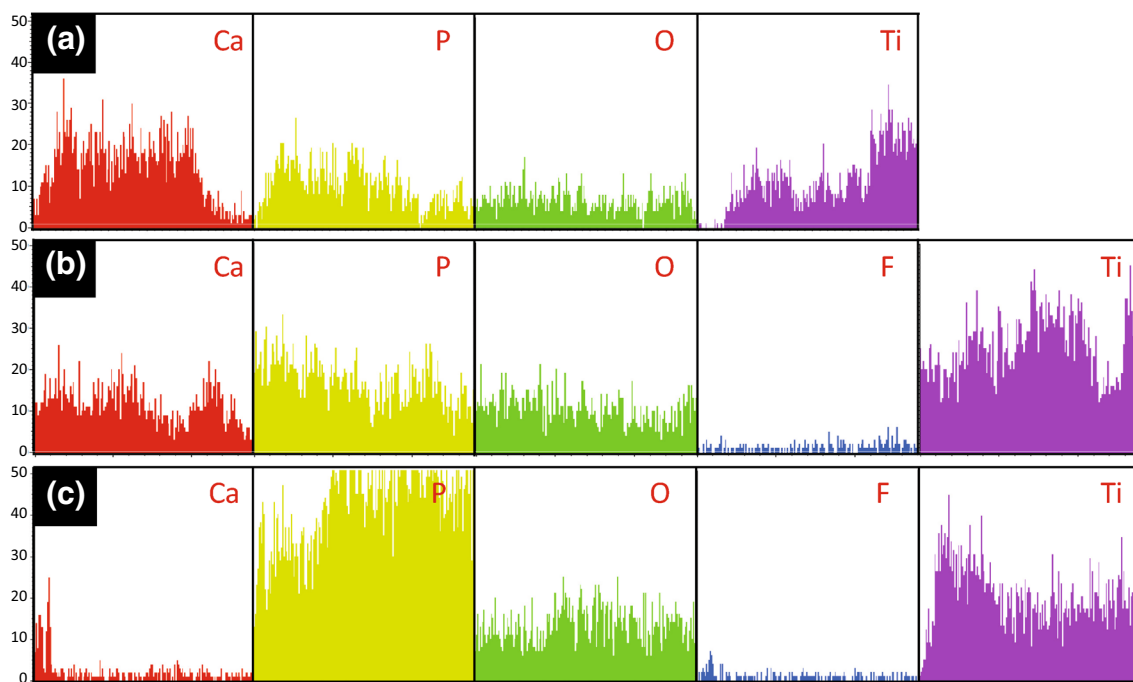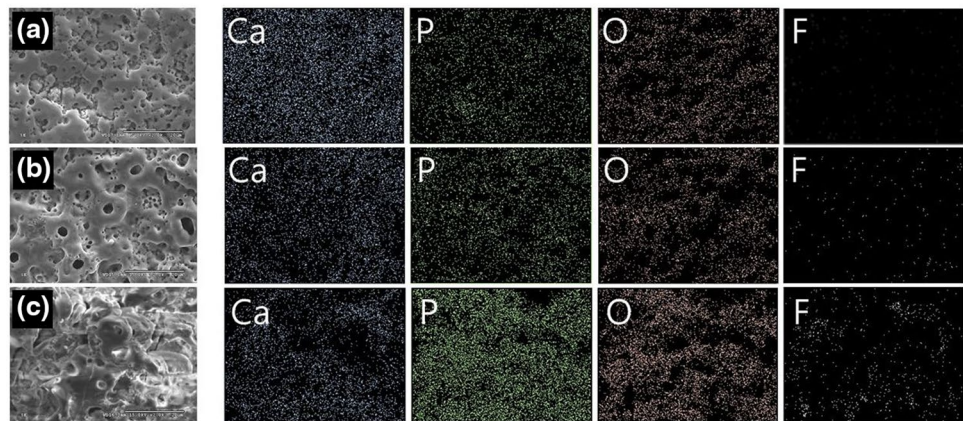

Fig. 4 EDS line scan results for Ca, P, O, F, and Ti contents across coating thickness. **a** 0%F, **b** 33%F, and **c** 67%F

of the coatings reduces from 3.95 to 0.42 as the F content is increased. Huang [27] reported that the Ca/P ratio of HA coatings deposited on pure Ti substrates using MAO is insensitive to the anodizing voltage and has a constant value of around 2.6. However, Chen [26] and Zhao [34] reported Ca/P ratio values of approximately 1.6 (similar to that of bone apatite). In practice, the Ca/P ratio of MAO films is dependent on both the synthesis parameters (i.e., the anodizing voltage and oxidation time) and the composition and concentration of the electrolyte.

Figure 5 presents the XRD spectra of the MAO coatings with 0%F, 33%F, and 67%F, respectively. It is seen that, apart from Ti, the 0%F coating contains HA, A-TiO$_2$

(Anatase), and R-TiO$_2$ (Rutile). Similarly, the 33%F specimen contains A-TiO$_2$, R-TiO$_2$, and a small amount of HA. Finally, the 67%F coating consists of Ti, A-TiO$_2$, R-TiO$_2$, CaF$_2$, TiP$_2$O$_5$, and FA. In general, the results show that the addition of CaF$_2$ to the MAO electrolyte contributes to the formation of FA phase in the coatings. Wang [35] prepared fluoridated HA coatings on Ti substrates using an electrochemical technique with a mixed solution of Ca(NO$_3$)$_2$, NH$_4$H$_2$PO$_4$, NaNO$_3$, and H$_2$O$_2$. In performing the electrolysis process, NaF was added to the solution to increase the concentration of F$^-$ ions and enhance FA generation. However, a post-treatment of the electrodeposited coatings was still required to complete the formation of apatite
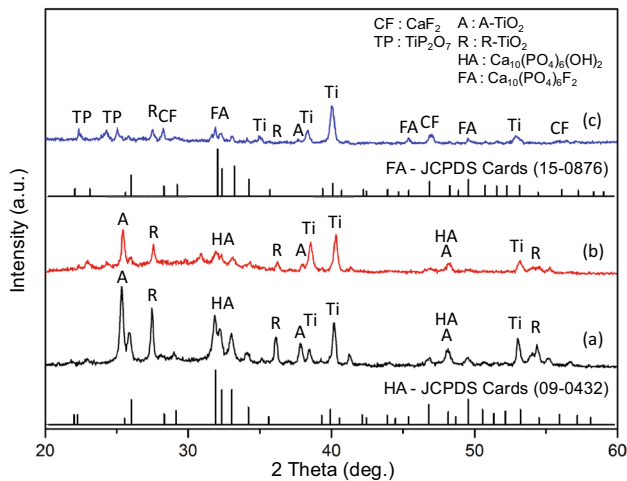
Fig. 5 XRD patterns of coatings prepared using electrolyte solutions with *a* 0%F, *b* 33%F, and *c* 67%F

Fig. 6 Surface micro-hardness and porosity of coated and uncoated Cp-Ti substrates

structures. In the MAO process performed in this study, an increasing quantity of CaF_2 in the electrolyte solution increases the F^- ion concentration, but decreases the OH^- ion concentration. Since the F^- ion radius is smaller than the OH^- ion radius, the OH^- ions are easily replaced by the F^- ions, prompting a reaction with the specimen surface and the direct formation of FA. Furthermore, the MAO process is performed using a high anodizing voltage, and hence, the specimen surface reaches the temperature required to achieve sintering, thereby further promoting the formation of FA.

For the electrolyte with the lowest F content (0%), the solution contains only $Ca(CH_3COO)_2 \cdot H_2O$ and $NaH_2PO_4 \cdot 2H_2O$. Thus, the coating surface has only HA, A-TiO_2 and R-TiO_2 phases (i.e., no FA). The authors in [24, 28] showed that as the MAO anodizing voltage or discharge duration time increases, the intensity of the R-TiO_2 phases increases, while that of the A-TiO_2 phases decreases. Furthermore, as the applied voltage or discharge duration time is further increased, the A-TiO_2 and R-TiO_2 phases are gradually replaced by HA phase. For the 33%F sample prepared in this study, the electrolyte solution contains 0.13 M CaF_2. However, the coating contains only A-TiO_2, R-TiO_2, and a small amount of HA phase. In other words, FA is still not formed, since the CaF_2 concentration of the electrolyte is insufficiently high to produce the F^- ions required to generate FA. For the 67%F sample, the CaF_2 concentration of the electrolyte reaches its maximum value (0.26 M), while that of $Ca(CH_3COO)_2 \cdot H_2O$ reaches its minimum value (0 M). As a result, the electrolyte solution contains only CaF_2 and $NaH_2PO_4 \cdot 2H_2O$ in a concentration ratio of 2:1. Under this condition, the CaF_2 concentration of the electrolyte is sufficiently high to generate FA directly following the MAO reaction. Furthermore, due to its high content, the
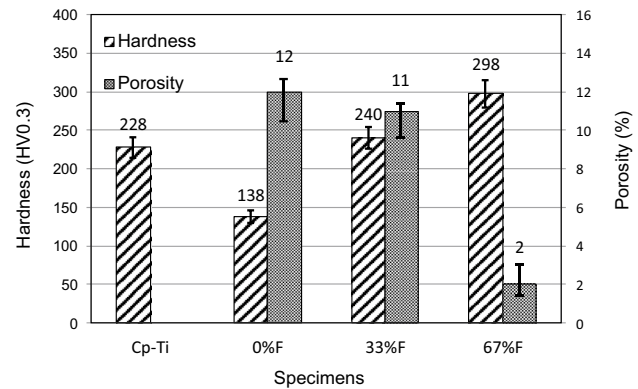
CaF_2 is not fully dissolved in the electrolyte solution and is thus partly deposited directly in the oxide layer. In addition, TiP_2O_5 is formed as a result of a reaction between the $NaH_2PO_4 \cdot 2H_2O$ content in the electrolyte solution and the Ti substrate.

3.2 Micro-hardness and porosity of MAO coatings

Figure 6 shows the micro-hardness and porosity values of the original Cp-Ti substrate and the various MAO coatings, respectively. Note that for each sample, the hardness was measured at 20 individual points and the results were then averaged to obtain a single representative value. It is seen that the coating hardness increases with an increasing CaF_2 content. For the 0%F sample (composed of HA, A-TiO_2 and R-TiO_2 phases), the hardness is significantly lower than that of the substrate. For the 33%F sample (composed of A-TiO_2, R-TiO_2, and a small amount of HA), the hardness is similar to that of the substrate. Finally, for the 67%F sample (consisting of A-TiO_2, R-TiO_2, CaF_2, TiP_2O_5, and FA phase), the hardness is notably higher than that of the substrate. When compared the porosity of samples shown in Fig. 6, it is revealed that the hardness reduces with an increasing porosity. Since the degree of surface porosity affects the hardness and also the elastic modulus of the coating [29], which can even be further tailored to match the modulus of bone, thus reducing the problems associated with stress shielding [36].

3.3 In vitro bioactivity of MAO coatings following immersion in SBF

Figure 7 presents SEM surface morphology images of the three MAO coating samples following prolonged immersion (7–28 days) in SBF. It can be seen that some bone-like apatite granules have been formed on the surfaces after 7-day immersion in SBF, and increasing gradually with

Fig. 7 Surface morphologies of specimens soaked in SBF for periods of 7–28 days. **a** 0%F, **b** 33%F, and **c** 67%F
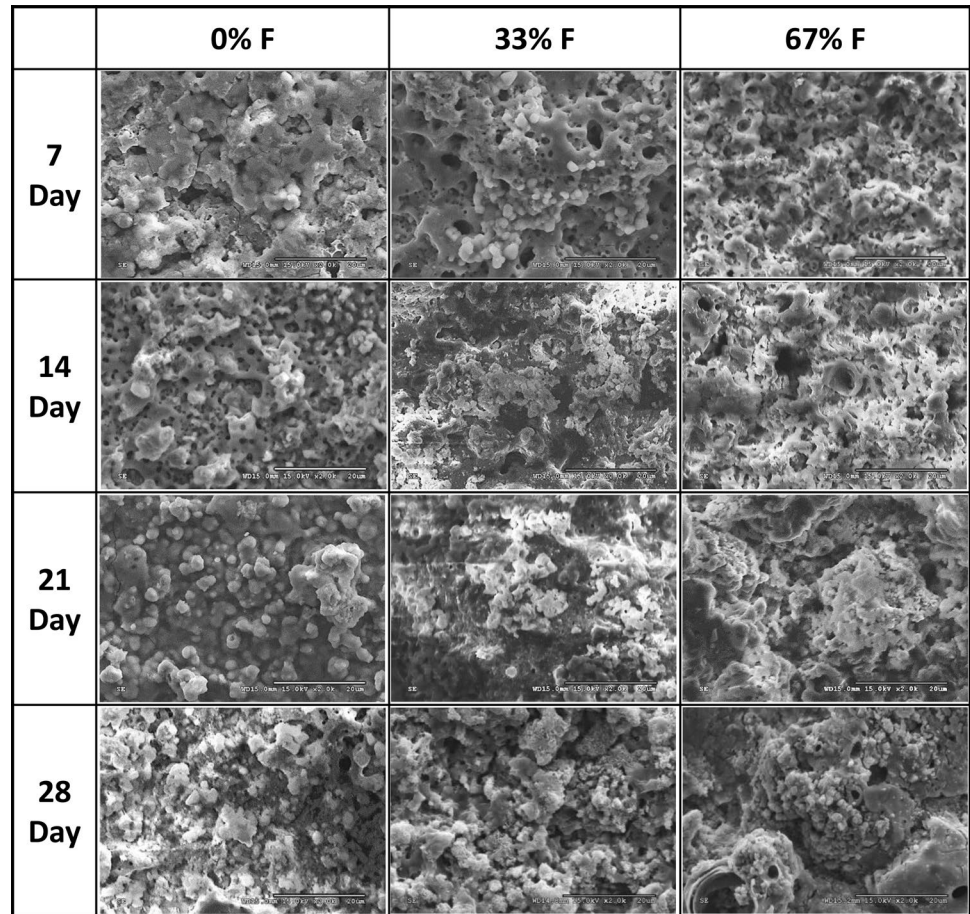
the period of time. The bone-like apatite formability of all three samples did not show evident difference after 28-day immersion in SBF. The porous surfaces produced by the MAO process here can provide a certain degree of in vitro bioactivity performance.

The XRD patterns of the specimen surfaces are shown in Fig. 8 and reveal that the A-TiO$_2$ and R-TiO$_2$ phases in the original coatings are still present following SBF immersion. In addition, all three spectra contain apatite peaks. However, the spectra also contain strong Ti peaks, which indicates that the bone-like apatite does not fully cover the MAO specimen surface.

In addition to the formation of a porous surface, which is favorable to osseointegration, the MAO processing technique, when performed with appropriate electrolyte solutions or combined with other treatments (e.g., hydrothermal treatment), also contributes to the formation of bioactive and biocompatible coatings. Chung [37] and Lee [38] added different proportions of strontium (Sr) ions to the electrolyte used in the MAO process, and showed that while Sr addition had a little effect on the mechanical properties of the coating (in the absence of further heat treatment), the bioactivity of the coating was significantly improved.
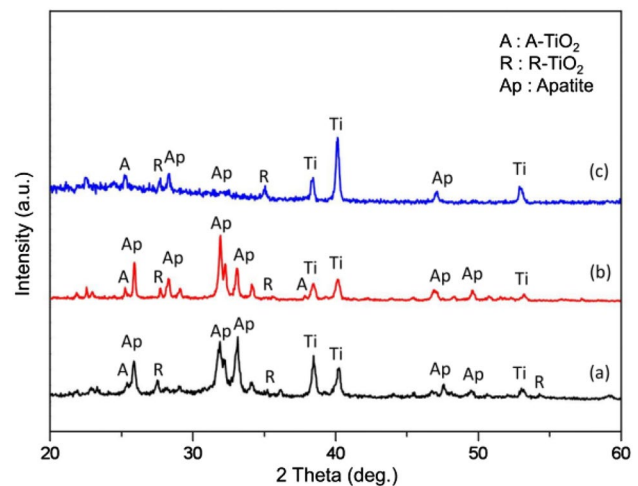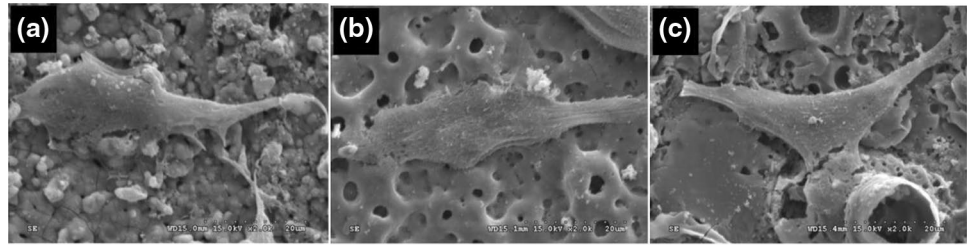

Fig. 8 XRD patterns of specimens soaked in SBF for 28 days. *a* 0%F, *b* 33%F, and *c* 67%F

3.4 Initial investigation into in vitro biocompatibility of MAO coatings

Figure 9 shows SEM images showing the morphologies of the MG63 cells incubated for 24 h on the MAO coatings

Fig. 9 SEM images of MG63 cells cultured on coated specimens for 24 h. **a** 0%F, **b** 33%F, and **c** 67%F

with 0%F, 33%F, and 67%F, respectively. It is observed that cell attachment and spreading occur on all three specimens. Moreover, as the $CaF_2/Ca(CH_3COO)_2 \cdot H_2O$ ratio (i.e., F content) of the MAO electrolyte solution increases, the degree of spreading also increases slightly. The biologic response of osteogenic cells is strongly dependent on the surface properties [39]. For example, cell attachment and spreading, both important indicators of the biocompatibility of a biomaterial, are governed by the composition, chemical states, and morphology of the surface [27]. Many methods have been proposed for improving the biocompatibility of Ti implants by modifying the surface composition and surface morphology. However, the MAO technique used in this study combines chemical and morphological modification of the Ti surface in a single step, and is a simple, controllable, and cost-effective method compared to other techniques, such as plasma spraying [40].

Chung [37] and Kung [40] showed that the biological performance of MAO coatings can be enhanced by incorporating strontium, calcium, and phosphorus ions into the coating material by means of an appropriate control of the composition and concentration of the electrolyte solution. Similarly, it was shown in [41] that the presence of strontium, calcium, and phosphorus is beneficial in promoting the precipitation of apatite and inducing a greater attachment and spreading of MG63 osteoblast-like cells on pure Ti substrates. The previous studies [42–45] have shown that surface modification affects both cell proliferation and cell differentiation. More specifically, as the surface roughness increases, the cell proliferation rate decreases, while the alkaline phosphatase (ALP) activity increases. Furthermore, while cell differentiation is sensitive to the chemical composition of the modified surface, cell proliferation is not [45].

As discussed in Sect. 3.1, the 0%F and 33%F samples contain large quantities of $R\text{-}TiO_2$, $A\text{-}TiO_2$, and HA phases, where the HA phase consists of Ca- and P-containing compounds. Although the richest F specimen (67%) has no HA phases, it consists of FA, which also contains Ca- and P-containing compounds. The previous studies have found no statistical difference in the cell growth abilities of HA and FA under similar surface conditions [46, 47]. However, the present results appear to show that the surface composition (or some other property) of the MAO coating has

a slight effect on the attachment and spreading of MG63 cells.

As shown in Fig. 6, the 0%F and 33%F coatings have average micropore diameters of around 1–2 and 3–5 μm, respectively, and are thus compatible with the pore size required to facilitate new bone growth (around 2–10 μm [48]). However, the porosities of the two samples, i.e., 12% and 11%, respectively, are much higher than that of the 67%F specimen (~2%). In other words, relatively speaking, they have a much higher surface roughness, and are thus less conducive to cell proliferation [42–45]. Consequently, a slight improvement in the cell spreading area is observed in the 67%F sample.

Xie [49] showed the cellular behaviors of nanocrystalline β-Ti alloy and revealed that along with the combination of high hardness and low Young's modulus, it exhibited excellent cell attachment and cell proliferation. However, in our study, although the hardness of three specimens has obviously differences, it is hardly found that how it affects the cellular behaviors from the results of the initial in vitro biocompatibility test.

Overall, the present results show that all three MAO coatings exhibit a reasonable in vitro bioactivity and biocompatibility performance. Furthermore, a slight improvement in the biocompatibility occurs as the $CaF_2/Ca(CH_3COO)_2 \cdot H_2O$ ratio (F content) of the MAO electrolyte solution increases. F content has limited effect on improving the cell growth ability. However, the MAO coating of the richest F specimen (67%) will lead to the formation of FA; its chemical and thermal stabilities are better than those of HA [10–12]. It is suggested that the formation of FA on the specimen surface is beneficial for biomedical applications.

4 Conclusions

This study has examined the surface morphology, composition, micro-hardness, and biological properties of bioceramic layers prepared on pure titanium substrates using an MAO process with three different electrolyte solutions containing calcium fluoride (CaF_2), calcium acetate monohydrate ($Ca(CH_3COO)_2 \cdot H_2O$), and sodium phosphate monobasic dihydrate ($NaH_2PO_4 \cdot 2H_2O$) mixed in ratios

of 0:2:1, 1:1:1, and 2:0:1, respectively. The experimental results support the following main conclusions.

1. As the proportion of $CaF_2/Ca(CH_3COO)_2 \cdot H_2O$ in the electrolyte solution increases, the main components of the coating (other than Ti) transform from HA, A-TiO$_2$, and R-TiO$_2$: into A-TiO$_2$, R-TiO$_2$ and a small amount of HA; and finally into A-TiO$_2$, R-TiO$_2$, CaF$_2$, TiP$_2$O$_5$, and FA. In other words, the addition of CaF$_2$ to the MAO electrolyte is beneficial in prompting the formation of FA in the coating.

2. As the $CaF_2/Ca(CH_3COO)_2 \cdot H_2O$ content in the electrolyte increases, the micro-hardness of the MAO coatings increases, while the porosity decreases. The hardness of the 67%F specimen is higher than that of the uncoated Cp-Ti substrate. However, due to its lower porosity, the surface roughness of the 67%F specimen is relatively lower than that of the 0%F and 33%F specimens.

3. Apatite is formed on the surfaces of all three specimens following prolonged (28 days) immersion in SBF. In other words, all three specimens have a certain degree of in vitro bioactivity despite being prepared using different proportions of $CaF_2/Ca(CH_3COO)_2 \cdot H_2O$ in the electrolyte.

4. For all three specimens, attachment and spreading of MG63 cells occur on the coating surface following incubation for 24 h. A slightly improved cell response is observed with an increasing $CaF_2/Ca(CH_3COO)_2 \cdot H_2O$ ratio (fluoride content) of the MAO electrolyte solution. The slight improvement in the biocompatibility of the 67%F coating can be attributed mainly to a reduction in the surface roughness (i.e., a lower micro-porosity) as the FA content increases.

References

1. L. Sennerby, P. Thomsen, L.E. Ericson, Ultrastructure of the bone-titanium interface in rabbits. J. Mater. Sci. Mater. Med. **3** (4), 262–271 (1992).

2. D.E. Steflif, A.L. Sisk, G.R. Parr, L.K. Garner, P.J. Hanes, F.T. Lake, D.J. Berkery, P. Brewer, Osteogenesis at the dental implant interface: high-voltage electron microscopic and conventional transmission electron microscopic observations. J. Biomed. Mater. Res **27**(6), 791–800 (1993)

3. C.S. Chien, T.Y. Liao, T.F. Hong, T.Y. Kuo, C.H. Chang, M.L. Yeh, T.M. Lee, Surface microstructure and bioactivity of hydroxyapatite and fluorapatite coatings deposited on Ti-6Al-4V substrates using Nd-YAG laser. J. Med. Biol. Eng. **34** (2), 109–115 (2014).

4. C.S. Chien, Y.S. Ke, T.Y. Kuo, T.Y. Liao, T.M. Lee, T.F. Hong, Effect of TiO$_2$ addition on surface microstructure and bioactivity of fluorapatite coatings deposited using Nd:YAG laser. Proc. Inst. Mech. Eng. H. **228** (4), 379–387 (2014).

5. C.S. Chien, T.Y. Liao, T.F. Hong, T.Y. Kuo, J.L. Wu, T.M. Lee, Investigation into microstructural properties of fluorapatite Nd-YAG laser clad coatings with PVA and WG binders. Surf. Coat. Technol **205**(10), 3141–3146 (2011)

6. C.S. Chien, T.F. Hong, T.J. Han, T.Y. Kuo, T.Y. Liao, Effects of different binders on microstructure and phase composition of hydroxyapatite Nd–YAG laser clad coatings. Appl. Surf. Sci **257**(6), 2387–2393 (2011)

7. T.F. Hong, Z.X. Guo, R. Yang, Fabrication of porous titanium scaffold materials by a fugitive filler method. J. Mater. Sci. Mater. Med. **19**, 3489–3495 (2008).

8. C.Y. Yang, T.M. Lee, Y.Z. Lu, C.W. Yang, T.S. Lui, A. Kuo, B.W. Huang, The influence of plasma-sprayed parameters on the characteristics of fluorapatite coatings. J. Med. Biol. Eng. **30** (2), 91–98 (2010).

9. S.C. Mojumdar, J. Kozánková, J. Chocholoušek, J. Majling, D. Fábryová, Fluoroapatite—material for medicine, growth, morphology and thermoanalytical properties. J. Therm. Anal. Cal. **78** (1), 73–82 (2004).

10. Y. Chen, X. Mian, Thermal and chemical stability of fluorohydroxyapatite ceramics with different fluorine contents. Biomaterials **26**(11), 1205–1210 (2005)

11. F.B. Ayed, J. Bouaziz, Sintering of tricalcium phosphate–fluorapatite composites by addition of alumina. Ceram. Int. **34** (8), 1885–1892 (2008).

12. K.A. Bhadang, K.A. Gross, Influence of fluorapatite on the properties of thermally sprayed hydroxyapatite coatings. Biomaterials **25**(20), 4935–4945 (2004)

13. Al-Noaman, N. Karpukhina, S.C.F. Rawlinson, R.G. Hill, Effect of FA on bioactivity of bioactive glass coating for titanium dental implant. Part I: Composite powder. J. Non Cryst. Solids. **364**, 92–98 (2013).

14. W.J. Dhert, C.P. Klein, J.A. Jansen, E.A. van der Velde, R.C. Vriesde, P.M. Rozing, K. de Groot, A histological and histomorphometrical investigation of fluorapatite, magnesiumwhitlockite, and hydroxylapatite plasma-sprayed coatings in goats. J. Biomed. Mater. Res **27**(1), 127–138 (1993)

15. C.P.A.T. Klein, J.G.C. Wolke, J.M.A. De Blieck-Hogervorst, K. de Groot, Calcium phosphate plasma-sprayed coatings and their stability: an in vivo study. J. Biomed. Mater. Res **28**(8), 909–917 (1994)

16. M. Wei, J.H. Evans, T. Bostrom, L. Grøndahl, Synthesis and characterization of hydroxyapatite, fluoride-substituted hydroxyapatite and fluorapatite. J. Mater. Sci. Mater. Med. **14** (4), 311–320 (2003).

17. X. Zheng, M. Huang, C. Ding, Bond strength of plasma-sprayed hydroxyapatite/Ti composite coatings. Biomaterials **21**(8), 841–849 (2000)

18. S.W.K. Kweh, K.A. Khor, P. Cheang, An in vitro investigation of plasma sprayed hydroxyapatite (HA) coatings produced with flame-spheroidized feedstock. Biomaterials **23**(3), 775–785 (2002)

19. W. Weng, J.L. Baptista, Preparation and characterization of hydroxyapatite coatings on Ti6Al4V alloy by a sol-gel method. J. Am. Ceram. Soc. **82**(1), 27–32 (1999)

20. O. Blind, L.H. Klein, B. Dailey, L. Jordan, Characterization of hydroxyapatite films obtained by pulsed-laser deposition on Ti and Ti-6Al-4V substrates. Dent. Mater. **21** (11), 1017–1024 (2005).

21. M.C. Kuo, S.K. Yen, The process of electrochemical deposited hydroxyapatite coatings on biomedical titanium at room temperature. Mater. Sci. Eng. C **20**(1–2), 153–160 (2002)

22. A.L. Yerokhin, X. Nie, A. Leyland, A. Matthews, S.J. Dowey, Plasma electrolysis for surface engineering. Surf. Coat. Technol **122**(2–3), 73–93 (1999)

23. W.F. Cui, L. Jin, L. Zhou, Surface characteristics and electrochemical corrosion behavior of a pre-anodized microarc oxidation coating on titanium alloy. Mater. Sci. Eng. C **33**(7), 3775–3779 (2013)

24. J.H. Ni, Y.L. Shi, F.Y. Tan, J.Z. Chen, L. Wang, Preparation of hydroxyapatite-containing titania coating on titanium substrate by micro-arc oxidation. Mater. Res. Bull **43**(1), 45–53 (2008)

25. X.L. Shi, Q.L. Wang, F.S. Wang, S.R. Ge, Effects of electrolytic concentration on properties of micro-arc film on Ti6Al4V alloy. Mini. Sci. Technol. **19** (2), 220–224 (2009).

26. J.Z. Chen, Y.L. Shi, L. Wang, F.Y. Yan, F.Q. Zhang, Preparation and properties of hydroxyapatite-containing titania coating by micro-arc oxidation. Mater. Lett **60**(20), 2538–2543 (2006)

27. Y. Huang, Y. Wang, C. Ning, K. Nan, Y. Han, Hydroxyapatite coatings produced on commercially pure titanium by micro-arc oxidation. Biomed. Mater. **2** (3), 196–201 (2007).

28. L.T. Duarte, C. Bolfarini, S.R. Biaggio, R.C. Rocha-Filho, P.A. Nascente, Growth of aluminum-free porous oxide layers on titanium and its alloys Ti-6Al-4V and Ti-6Al-7Nb by micro-arc oxidation. Mater. Sci. Eng. C **41**, 343–348 (2014)

29. G. Ryan, A. Pandit, D.P. Apatsidis, Fabrication methods of porous metals for use in orthopaedic applications. Biomaterials. 27(13), 2651–2670 (2006).

30. M. Mour, D. Das, T. Winkler, E. Hoenig, G. Mielke, M.M. Morlock, A.F. Schilling, Advances in porous biomaterials for dental and orthopaedic applications. Materials, 3, 2947–2974 (2010).

31. M.R. Bayati, F. Golestani-Fard, A.Z. Moshfegh, How photocatalytic activity of the MAO-grown TiO$_2$ nano/micro-porous films is influenced by growth parameters? Appl. Surf. Sci **256**(13), 4253–4259 (2010)

32. X.F. Xiao, R.F. Liu, Effect of suspension stability on electrophoretic deposition of hydroxyapatite coatings. Mater. Lett **60**(21–22), 2627–2632 (2006)

33. F.A. Akin, H. Zreiqat, S. Jordan, M.B.J. Wijesundara, Preparation and analysis of macroporous TiO$_2$ films on Ti surfaces for bone–tissue implants. J. Biomed. Mater. Res **57**(4), 588–596 (2001)

34. Q.M. Zhao, H.L. Yang, Z.T. Liu, X.F. Gu, C. Li, D.H. Feng, Fabrication of hydroxyapatite on pure titanium by micro-arc oxidation coupled with microwave-hydrothermal treatment. J. Mater. Sci. Mater. Med. **26** (88), 1–8 (2015).

35. J. Wang, Y. Chao, Q. Wan, Z. Zhu, H. Yu, Fluoridated hydroxyapatite coatings on titanium obtained by electrochemical deposition. Acta Biomater **5**(5), 1798–1807 (2009)

36. H.U. Cameron, I. Macnab, R.M. Pilliar, A porous metal system for joint replacement surgery. Int. J. Artif. Organs. 1(2), 104–109 (1978).

37. C.J. Chung, H.Y. Long, Systematic strontium substitution in hydroxyapatite coatings on titanium via micro-arc treatment and their osteoblast/osteoclast responses. Acta Biomater **7**(11), 4081–4087 (2011)

38. T.M. Lee, K.C. Kung, K. Yuan, T.S. Lui, Effect of heat treatment on microstructures and mechanical behavior of porous Sr-Ca-P coatings on titanium. J. Alloy Compd **515**(25), 68–73 (2012)

39. M.J. Kim, C.W. Kim, Y.J. Lim, S.J. Heo, Microrough titanium surface affects biologic response in MG63 osteoblast-like cells. J. Biomed. Mater. Res. A. **79** (4), 1023–1032 (2006).

40. K.C. Kung, T.M. Lee, J.L. Chen, T.S. Lui, Characteristics and biological responses of novel coatings containing strontium by micro-arc oxidation. Surf. Coat. Technol **205**(6), 1714–1722 (2010)

41. Y. Nagai, C. Yamazaki, K. Ma, T. Nozaki, K. Toyamab, Yamashita, Response of osteoblast-like MG63 cells to TiO$_2$ layer prepared by micro-arc oxidation and electric polarization. J. Eur. Ceram. Soc **32**(11), 2647–2652 (2012)

42. W.H. Song, H.S. Ryu, S.H. Hong, Antibacterial properties of Ag (or Pt)-containing calcium phosphate coatings formed by micro-arc oxidation. J. Biomed. Mater. Res. A, **88** (1), 246–254 (2009).

43. J.Y. Martin, Z. Schwartz, T.W. Hummert, D.M. Schraub, J. Simpson, J. Lankford, D.D. Dean, D.L. Cochran, B.D. Boyan, Effect of titanium surface roughness on proliferation, differentiation, and protein synthesis of human osteoblast-like cells (MG63). J. Biomed. Mater. Res **29**(3), 389–401 (1995)

44. B.D. Boyan, R. Batzer, K. Kieswetter, Y. Liu, D.L. Cochran, S. Szmuckler-Moncler, D.D. Dean, Z. Schwartz, Titanium surface roughness alters responsiveness of MG63 osteoblast-like cells to 1 α,25-(OH)2D3. J. Biomed. Mater. Res **39**(1), 77–85 (1998)

45. L.H. Li, Y.M. Kong, H.W. Kim, Y.W. Kim, H.E. Kim, S.J. Heo, J.Y. Koak, Improved biological performance of Ti implants due to surface modification by micro-arc oxidation. Biomaterials **25**(14), 2867–2875 (2004)

46. H. Eslami, M. Solati-Hashjin, M. Tahriri, The comparison of powder characteristics and physicochemical, mechanical and biological properties between nanostructure ceramics of hydroxyapatite and fluoridated hydroxyapatite. Mater. Sci. Eng. C **29**(4), 1387–1398 (2009)

47. C.F. Dunne, B. Twomey, C. Kelly, J.C. Simpson, K.T. Stanton, Hydroxyapatite and fluorapatite coatings on dental screws: effects of blast coating process and biological response. J. Mater. Sci. Mater. Med. **26** (1), 1–14 (2015).

48. G.L. Darimont, R. Cloots, E. Heinen, L. Seidel, R. Legrand, In vivo behaviour of hydroxyapatite coatings on titanium implants: a quantitative study in the rabbit. Biomaterials **23**(12), 2569–2575 (2002)

49. K.Y. Xie, Y. Wang, Y. Zhao, L. Chang, G. Wang, Z. Chen, Y. Cao, X. Liao, E.J. Lavernia, R.Z. Valiev, B. Sarrafpour, H. Zoellner, S.P. Ringer, Nanocrystalline β-Ti alloy with high hardness, low Young's modulus and excellent in vitro biocompatibility for biomedical applications. Mater. Sci. Eng. C **33**(6), 3530–3536 (2013)